R-Matrix calculations for opacities: IV.: Convergence, completeness, and comparison of relativistic R-matrix and distorted wave calculations for Fe XVII and Fe XVIII

L Zhao[1], S N Nahar[1], A K Pradhan[1,2,3]

[1] Department of Astronomy, Ohio State University, Columbus, Ohio 43210, USA
[2] Biophysics Graduate Program, [3] Chemical Physics Program, The Ohio State University, Columbus, Ohio 43210, USA

Abstract. To investigate the completeness of coupled channel (CC) Breit-Pauli R-Matrix (BPRM) calculations for opacities, we employ the relativistic distorted wave (RDW) method to complement ("top-up") and compare the BPRM photoionization cross sections for high-$n\ell$ levels of both Fe XVII and Fe XVIII . Good agreement is found in background photoionization cross sections using these two methods, which also ensures correct matching of bound level cross sections for completeness. In order to top-up the CC-BPRM calculations, bound-bound transitions involving additional bound levels, and a large number of doubly-excited quasi-bound levels corresponding to BPRM autoionizing resonances described in paper RMOPII, are calculated using the RDW method. Photoionization cross sections in the high energy region are also computed and compared up to about 500 Ry, and contributions from higher core level excitations than BPRM are considered. The effect of configuration interaction is investigated, which plays a significant role in correctly reproducing some background cross sections. Owing to the fact that the additional RDW levels correspond to high-$n\ell$ bound levels that are negligibly populated according to the Mihalas-Hummer-Däppen equation-of-state (paper I), the effect on opacities is expected to be small.

1. Introduction

Previous papers I-III in this series (hereafter RMPP1, RMOP2, RMOP3) reported BPRM calculations and plasma effects related to iron opacity at conditions similar to the solar radiation/convection zone boundary or the base of the convection zone (BCZ). As outlined in paper RMOP1, opacity calculations need to consider all possible mechanisms for photon absorption and scattering from all atomic constituents, including all levels that might possibly contribute. Furthermore, in order to resolve discrepancies among various theoretical models based on the DW methods that include different sets of transition arrays, and experimental measurements [1, 2], it is necessary to establish convergence of the BPRM calculations and completeness of transitions considered.

Extensive CC-BPRM calculations *R*-Matrix (BPRM) calculations were carried out for Fe XVII including 60 fine-structure levels within the $n \leq 3$ complexes in the Fe XVIII target ion [3], and 99 *LS* terms within $n \leq 4$ (99LS-RM). They show strong photon absorption due to core excitation, resulting in an increment of 35% in the Rosseland mean opacity over the Opacity Project (OP) data [4]. Whereas these previous calculations demonstrated that in the *R*-Matrix opacity calculations convergence of the close-coupling expansion was a necessary condition for accuracy, completeness of all possible excited configurations by additional contributions in the high-energy region still remains to be ascertained [4, 5, 6]. At BCZ conditions Fe XVII , Fe XVIII and Fe XIX are the three dominant iron ions. For example, at the measured iron opacity [2] and temperature and density T=2.1×10^6 and N$_e$=$3.1 \times 10^2 2$cc, the three ionization fractions are 0.19, 0.38 and 0.29, respectively [4].

In this paper, we consider the 218CC-BPRM calculation for Fe XVII and 276CC-BPRM calculation for Fe XVIII , as described in paper RMOP2. The additional or topup transitions for bound-bound and bound-free data are obtained from relativistic distorted wave (RDW) calculations using the flexible atomic code (FAC) [7]. In the following sections, the specifications of the 218CC- and 276CC-BPRM calculations of paper RMOP2 are summarized, followed by the top-up configurations and transitions calculated using FAC. To ensure data correspondence from FAC, a procedure of matching the bound levels from BPRM and FAC results is described, and the bound-bound and bound-free top-up calculations detailed afterwards.

A key step in the matching-topup procedure is level identification. Unlike atomic structure and DW calculations, BPRM calculations do not assign spectroscopic designations *a priori* and bound states are obtained only as eigenvalues of the (e + ion) Hamiltonian. As described in paper RMOP2, the code BPID (Fig. 1, RMOP-I) is used to obtain relevant parameters and for spectroscopic identification of levels computed in BPRM calculations. The RDW calculations of course have a pre-assigned identification based on initial set of electronic configurations specified in the configuration-interaction (CI) basis. In some instances exited level configuration mixing is such that one configuration does not dominate the wavefunction expansion of a given state and RDW and BPRM assignations do not match. It is then required to carefully examine level parameters such as quantum defects and associated bound-bound and bound-free transitions to ascertain matching data. Another consideration is that the precise number of BPRM bound-state eigenvalues depends on an energy mesh or effective quantum number $\nu(E)$ obtained by "scanning" at a fine mesh with sufficient refinement to ensure convergence. The procedure and results are discussed in this paper.

A potentially important factor is that the close coupling approximation introduces autoionizing resonances in photoionization cross section, which may be affected by radiative damping in highly charged H- or He-like ions, and thereby reduce effective cross sections considerably [16]. However, radiation damping occurs *after* photoabsorption, and for ions such as Fe XVII and Fe XVIII this effect is negligible [13, 14]. Therefore, undamped photoionization cross sections are used in opacity calculations, as reported

in paper RMOP2.

2. BPRM bound-free and bound-bound data

The current BPRM calculations for Fe XVII and Fe XVIII are unprecedented in terms of scope and magnitude of data produced and processed for opacity calculations, with the maximum number of free channels 998 and 1288 respectively, from calculations reported in RMOP2. For Fe XVII , 99LS-RM calculation [4] is extended to 218CC-BPRM by including the fine structure of the target states. The target configurations ($1s$ is always full, so omitted for brevity) included are $2s^2 2p^5$, $2s 2p^6$, $2s^2 2p^4 n\ell$, $2s 2p^5 n\ell$, $2p^6 3\ell'$, where $n = 3$, 4, and ℓ, $\ell' \leq 2$, which have 99 LS terms, or 218 fine structure levels. The continuum orbitals included are $\ell \leq 9$, and the number of continuum R-Matrix basis functions included is 20. The bound states are found by scanning the eigenvalues of the (e + ion) Hamiltonian on an effective quantum number ν up to $\nu \leq 10.1$ [8]. However, as mentioned above, unlike atomic structure calculations where electronic configurations are specified *a priori*, R-matrix calculations do not provide spectroscopic spin-orbital quantum number designations for the bound levels obtained, nor guarantee that all possible bound levels are found within the ν-range of interest.

To resolve the first issue, the computer program BPID [9] has been developed as part of the RM opacity codes described in paper P1. Using the code BPID one can identify most of the bound levels spectroscopically, albeit with a few remaining highly mixed levels undetermined (viz. [10]). That obstacle might be overcome by comparing some physical quantities of these levels calculated by an atomic structure code such as SUPERSTRUCTURE [11] and FAC [7], as for example for photoionization cross section to be described in the next section. The second issue depends on the scanning $\Delta - \nu$-mesh employed; $\Delta\nu = 0.001$ yields fewer bound levels in the 218CC-BPRM than 60CC-BPRM, so a finer step 0.0001 or 0.0005 is used in the region where levels are missing, which finally gives 464 bound levels, 10 more than 60CC-BPRM.

For the larger Fe XVIII case, two sets of BPRM calculations are done with different target configurations. One includes up to $n = 3$ target configurations, i.e. $2s^2 2p^4$, $2s 2p^5$, $2p^6$, $2s^2 2p^3 3\ell$, $2s 2p^4 3\ell$, where $\ell \leq 2$, which yields 200 target fine structure levels. In addition to target configurations above, the other BPRM calculation includes $n = 4$ configurations, i.e. $2s^2 2p^3 4\ell$, where $\ell \leq 2$, which yield 276 fine structure levels. The parameters set for the continuum orbitals and basis functions are the same as for Fe XVII 218CC-BPRM calculation. The 200CC-BPRM calculation finds 1149 bound levels with $\Delta\nu = 0.001$, while 276CC-BPRM calculation finds 1163 bound levels with 0.001 as the initial attempt in ν-mesh, and 0.0001 or 0.0005 as the second attempt, in the region where levels are missing compared with 200CC-BPRM. Thus we may be confident of having converged with respect to possible number of bound levels with BPRM calculations.

To compute iron opacities for Fe XVII and Fe XVIII oscillator strengths from the 60CC-BPRM and 200CC-BPRM calculations, and photoionization cross sections

Table 1. Selected packed levels of Fe XVII ($J = 4, \pi = 0$) and Fe XVIII ($J = 5/2, \pi = 0$) (Note: the energy is z-scaled, and in unit of $10^{-2}Ry$)

	level index	60CC-BPRM	218CC-BPRM
Fe XVII	23	-1.242945	-1.239702
	24	-1.239540	-1.238049
	25	-1.237855	-1.236506
	26	-1.236421	-1.235733
	27	-1.235081	-1.235227
	28	-1.234742	-1.234723
	level index	200CC-BPRM	276CC-BPRM
Fe XVIII	31	-3.996445	-4.004678
	32	-3.993010	-4.003468
	33	-3.989362	-4.000058

from the 218CC-BPRM and 276CC-BPRM calculations, are used respectively (paper RMOP2). So in doing the FAC top-up calculations, matching the bound levels for each BPRM calculation is necessary but complicated by the fact that they have different number of bound levels, especially energy regions where levels are densely packed (see table 1) and the order of their spectroscopic designations may be mismatched and needs to be shuffled (see figure 1).‡ Photoionization cross sections of 6 levels of Fe XVII are plotted in figure 1 for 60CC-BPRM and 276CC-BPRM, and we find distinct difference in level 24 and 26. Similar issue arises in figure 1 of Fe XVIII . Even though these levels have similar energy, they may have distinctive configurations (see section 3.1), which is the reason why we should redo the identification for different CC-BPRM calculations. After being switched, these levels show good agreement (see figure 1).

3. Complementarity between BPRM and RDW: the top-up procedure

The Opacity Project [12] employed a small (e + ion) wavefunction expansion including outer open Shell configurations in the close-coupling approximation and *R*-Matrix method in LS-coupling to calculate non-relativistic photoionization cross sections in the low energy region, and adopted the Kramer approximation ("tail") to fit and extend to higher energies afterwards. In previous calculations, [13] replaced the Kramer tails with the RDW results including the contribution from inner-shell processes. Later opacity tables were updated by also including inner-shell transitions [15]. In this section, we describe the procedure employed to compare and complement BPRM data with RDW data from FAC. That requires careful matching between BPRM and FAC cross sections for all bound levels, and detailed bound-bound and bound-free top-up calculations. We

‡ It bears emphasis that the opacities *per se* are independent of any spectroscopic labels; however, they are necessary for processing the bound-bound and bound-free radiative atomic transitions, and for comparing with other data sources.
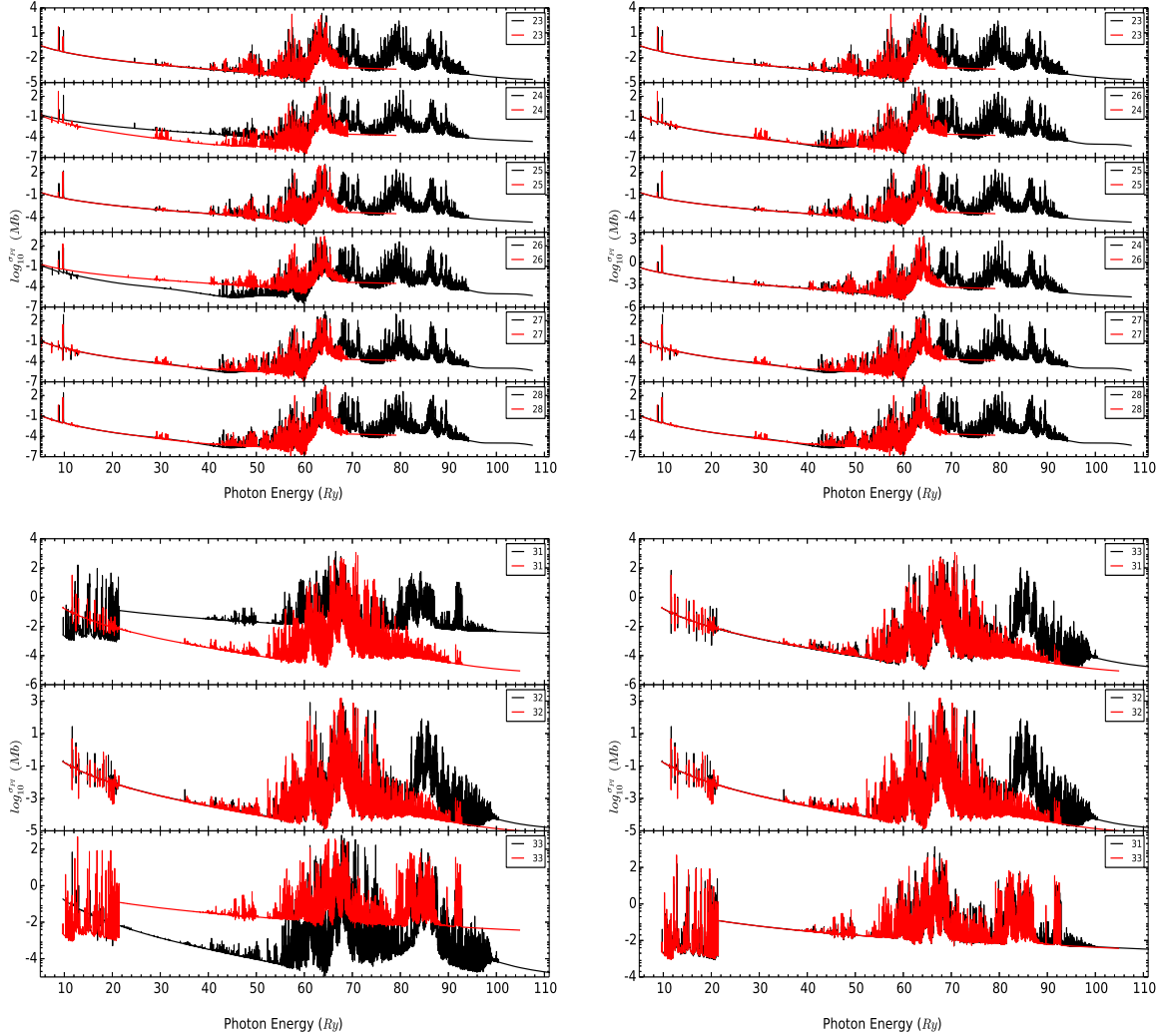
Figure 1. Photoionization cross section of 6 closely packed levels for Fe XVII and 3 levels for Fe XVIII before and after being switched. 60CC-BPRM (red), 218CC-BPRM (black); 200CC-BPRM (red), 276CC-BPRM (black)

also discuss the effect of configuration interaction on photoionization cross sections.

3.1. Matching

In BPRM calculations, bound levels with continuum orbitals $\ell \leq 9$ and effective quantum number $\nu \leq 10.1$ are formed by coupling the $n = 2$ core states with the continuum ν and ℓ of the outer electron. So in FAC we set the bound configurations as a permutation of the $n = 2$ core configurations and an outer electron with principle quantum number $n \leq 10$. With the same n-complex configuration interaction included, atomic structure is solved and sorted by total angular momentum J and parity π, and ordered in energy, we find excellent agreement in the energy between BPRM and FAC values.

In calculating photoionization cross sections we include the whole n-complex of

core configurations for CI (hereafter CI) purpose, but only the transitions to core configurations that are included in BPRM calculations. To delineate photoionization cross sections at the edges of energy grid, the energy mesh is created in such a way that within any two adjacent thresholds 10 points are uniformly assigned. The partial photoionization cross section is the computed in the default 6 energy grids, and interpolated/extrapolated in our mesh, and summed to give total cross sections for each bound level. To investigate the effect of CI, two sets of RDW calculation are carried out. Both sets only allow the same-n-complex configuration interaction for bound configurations, but for the core configurations one of them only allows the same-n-complex CI and the other allows different n-complexes. We mix all the core configurations together. In RDW calculations, the photoionization cross section is related to the dipole operator matrix $< \psi_i | \mathbb{D} | \psi_f >$. The $|\psi_i >$ involves the electron in the bound state to the continuum and all other electrons, and must stay the same if only same-n-complex configuration interaction is allowed. It can be different if different-n-complex CI is considered [7].

To match bound state levels from BPRM and RDW, it is necessary to compare cross sections to ensure the correctness of matching. We plot BPRM and RDW photoionization cross sections in the order of energy for each J, π symmetry pair, and a level is matched when the energy and the photoionization cross section agree reasonably well (here the background of the BPRM data and RDW are compared). Photoionization cross sections of majority of bound levels show excellent consistency at the first attempt (see figure 1 for Fe XVII and Fe XVIII . The LS-term notation (S and L) can not be determined from FAC output for all levels, so only configuration and total angular momentum J are given). However, when several levels are almost degenerate (see table 2), distinctive differences may yet occur in cross sections. Such levels need to be switched till good matching is achieved (See figure 3 for Fe XVII and Fe XVIII The process is justified since level identification of near-degenerate BPRM levels may not exactly correspond in energy from different atomic structure codes such as FAC, since spectroscopic designations depend on CI included and coupling schemes employed for the (e + ion) system§.

In table 2, we can see the energy levels computed in BPRM and RDW agree quite well. For Fe XVII , levels 13 and 14 , and levels 15 and 16 lie very close to each other, and in figure 3, levels 13 and 16 achieve good agreement, while levels 14 and 15 don't. So we switch the order of levels 14 and 15 in RDW calculation and recompare with good agreement. Thus levels 13 - 16 in BPRM calculation are matched with those in RDW calculation. The same procedure is applied to levels 65 and 66 of Fe XVIII in table 2, and the result is show in figure 3.

In figures 2 and 3, we show two sets of RDW calculation as described above, and study the effect of configuration interaction on photoionization cross sections, with the upper panel of figure 2 as an example. The dominant configuration of the bound state

§ All BPRM photoionization cross sections include a small region below the lowest ionization threshold for each level [12], where no RDW data are shown.

Table 2. Selected levels of Fe XVII ($J = 3, \pi = 1$) and Fe XVIII ($J = 1/2, \pi = 1$) to be matched (Note: the energy is z-scaled, and in unit of $10^{-2} Ry$)

	level index	BPRM	RDW
Fe XVII	12	-3.670657	-3.67960
	13	-2.873930	-2.84319
	14	-2.868775	-2.84238
	15	-2.842915	-2.83761
	16	-2.835625	-2.83555
	17	-2.774853	-2.77998
	level index	BPRM	RDW
Fe XVIII	64	-1.275887	-1.27703
	65	-1.234865	-1.24175
	66	-1.226084	-1.23724
	67	-1.136909	-1.14691

after being matched with RDW is $2s^2 2p^5 4d$, so with only the same-n-complex CI of core configurations considered, the transitions can only happen to core configurations $2s^2 2p^5$, $2s 2p^5 4\ell$, $2s^2 2p^4 4\ell$ and $2p^6 4\ell$, where $\ell = s, p, d$, while with different-n-complex CI of core configurations additional contribution can be from all other core configurations. From the upper panel of figure 2 we can see that the same-n-complex configuration interaction gives reasonably good background, though with some big gaps, while different-n-complex CI fills up the big gap and improves the background significantly. Similar phenomenon can be found in the rest of the figures 2 and 3, and there are still some gaps remaining after different-n-complex CI is allowed‖

3.2. Bound-free data

As BPRM calculations are carried out in the lower part of the whole energy range, they include low-$n\ell$ core configurations with $n \leq 4$. We use the RDW method to extend it to higher regions up to 500 Ry in photoelectron energy, and to include higher-$n\ell$ core configurations $n = 5, 6$. The following part of this section gives detailed description of these aspects.

3.2.1. High energy cross sections As shown in figure 2, the RDW data can be matched almost perfectly to background BPRM cross sections. However, we also find there are cases where they don't match well in the right region of energy (see figure 4). In the top panels different-n CI introduces many transitions, but they are not strong enough to raise to the background of BPRM. In the middle panel of figure 4, different-n CI introduces many edges at positions where the background of BPRM jumps, and raises

‖ In figure 2 and 3, the oscillation in the background of the BPRM data can be eliminated with a larger number of continuum basis functions [13].
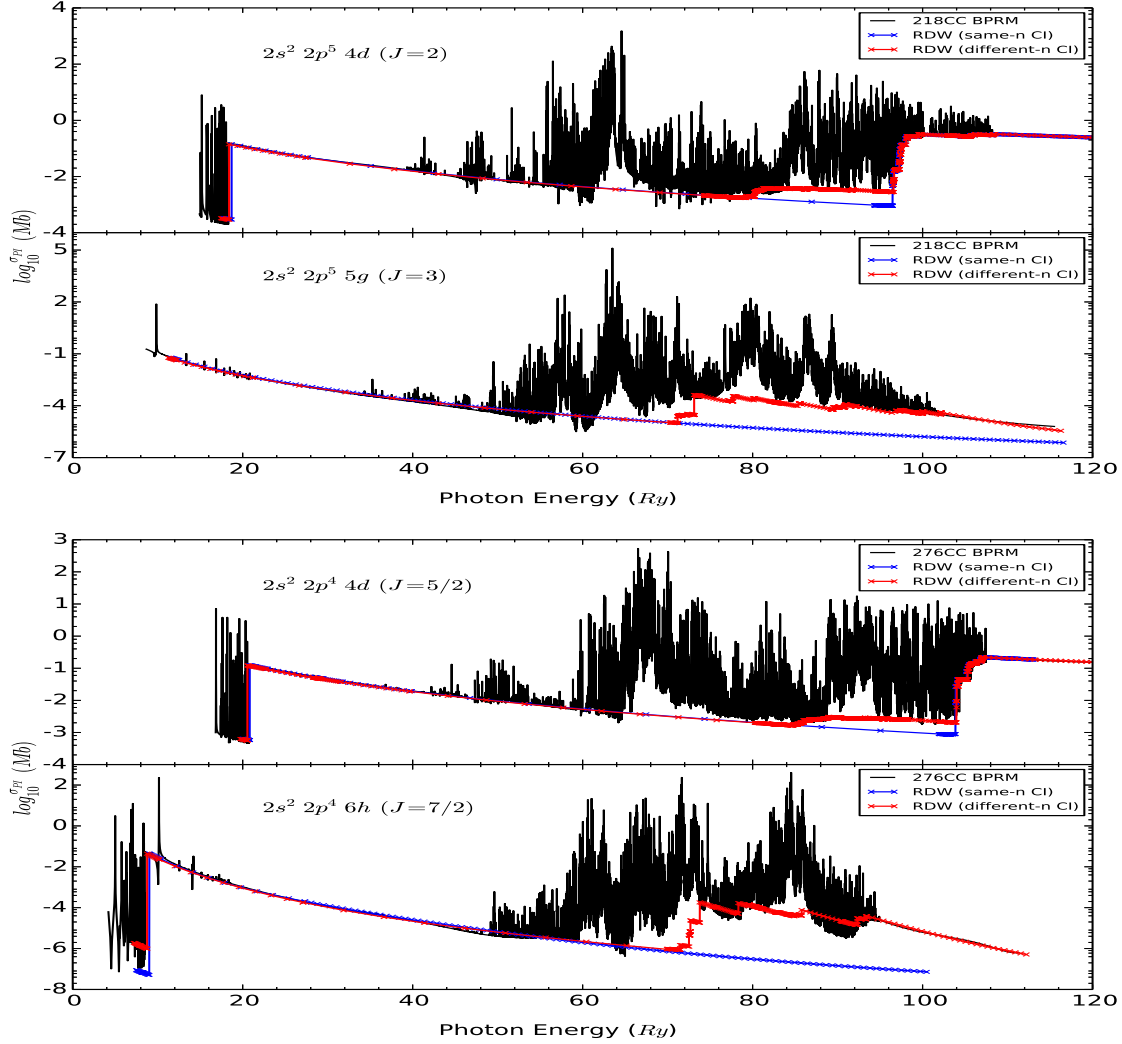
Figure 2. Most of the levels are matched at the first attempt with excellent consistency in photoionization cross section. The configuration is attached with each level. BPRM (black), RDW(blue and red). "Same-n CI" means only same-n-complex CI is considered for core configurations, and "different-n CI" refers to both same-n- and different-n-complex CI is considered.

the background higher than BPRM. While in the middle panel of figure 4, around $105Ry$, compared with same-n CI, different-n CI moves the background up on the left side, and down on the right side, i.e. converging to the background of BPRM. As close-coupling approximation treats CI more completely and accurately, we multiply the RDW data in the higher energy region by a factor which is the ratio of BPRM value and RDW value at the last point of BPRM calculation for each level (see figure 5), to account for the discrepancy between BPRM and RDW. In figure 5, the distribution of the factors applied in the higher region is very alike for Fe XVII and Fe XVIII , and there are around 60% of the bound levels lying around ratio $= 1$. Among the high-ratio cases, some are caused by the oscillation of the background of BPRM, which is due to the small number
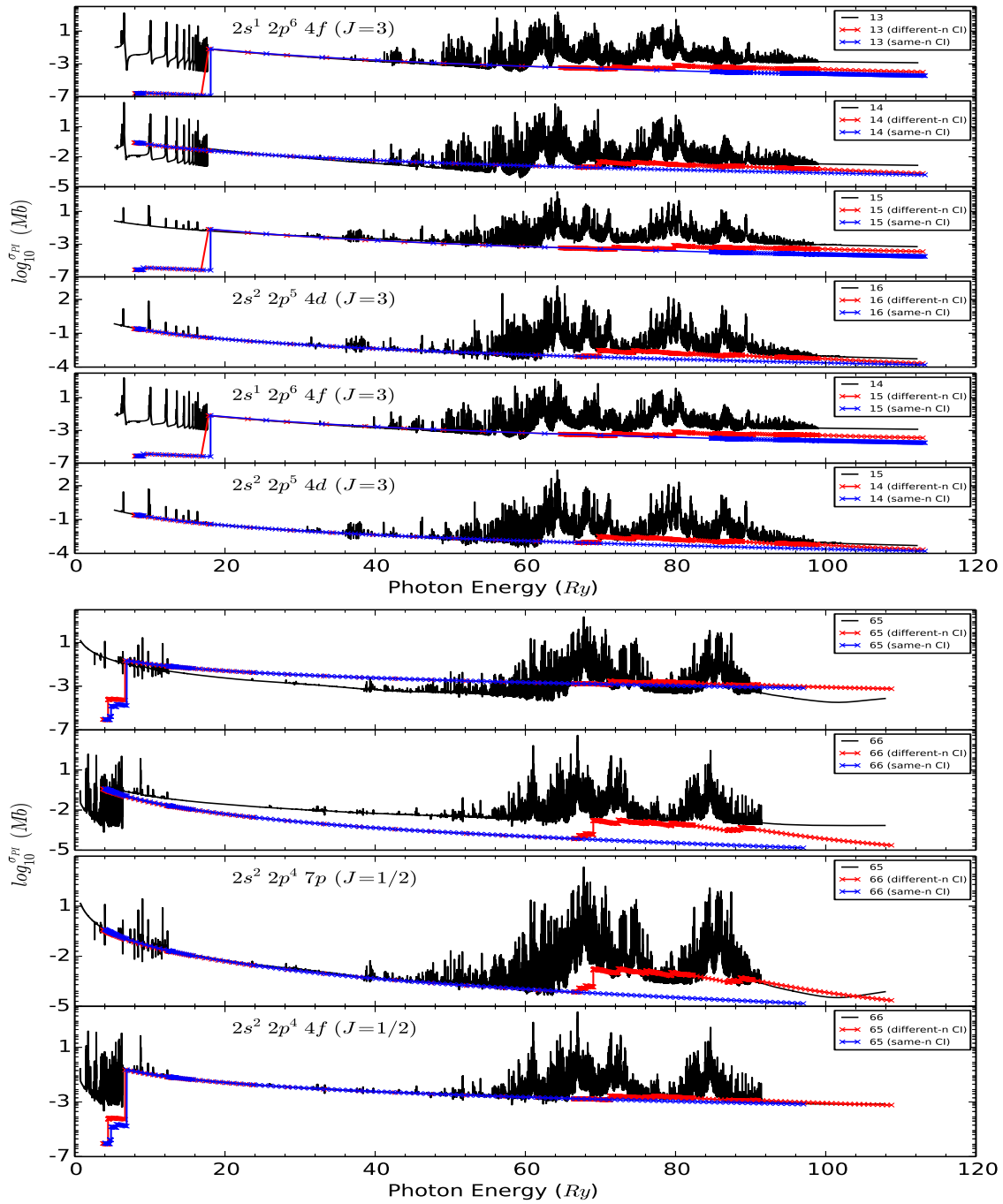
Figure 3. Multiple attempts are needed to ensure the correct matching when the levels are found with discrepancy in the photoionization cross section. In ?? and ?? the discrepancy is shown in upper panel and the final matching is in the lower one. Find the configuration attached for each level. BPRM (black), RDW(blue and red). "Same-n CI" refers to only same-n-complex CI is considered for core configurations, and "different-n CI" refers to both same-n- and different-n-complex CI are considered.

of continuum basis functions used in the wavefunction expansion [13] (see the bottom panels of figure 4.

The energy mesh used in the region is created in such a way that 10 points are uniformly assigned between any adjacent ionization thresholds due to the other core configurations (see section 3.2.2).

3.2.2. Highly excited core configurations   Using RDW with different-n-complex CI, we calculate photoionization cross section due to other core configurations up to $n = 6$ that are not included in the BPRM calculation. To top-up 218CC BPRM for Fe XVII , we include core configurations $2s^2 2p^4 4f$, $2s2p^5 4f$, $2p^6 4\ell'$, $2s^S 2p^P 5\ell''$ and $2s^S 2p^P 6\ell'''$, where ℓ', ℓ'', ℓ''' are all possible subshells in the corresponding shell, and s, p are any possible non-negative integers satisfying $S + P = 6$. To top-up 276CC BPRM for Fe XVIII , we include core configurations $2p^5 3\ell'$, $2s^2 2p^3 4f$, $2s2p^4 4\ell'$, $2p^5 4\ell''$, $2s^S 2p^P 5\ell'''$ and $2s^S 2p^P 6\ell''''$, where ℓ', ℓ'', ℓ''' and ℓ'''' are all possible subshells in the corresponding shell, and S, P are any possible non-negative integers satisfying $S + P = 5$. The energy mesh is same as the one used in BPRM calculation merged with the one in the high energy region as described in section **??**.

As shown in figure 6, the BPRM data is merged with the scaled RDW tail, and the contribute from other core configurations varies from negligible to noticeable.

3.2.3. Highly excited bound levels   In RDW, we consider all the bound state levels with $n \leq 10$, so we collect all such levels that are not included in BPRM calculation, and calculate the photoionization cross section due to all core configurations, i.e. the core configurations included in the BPRM calculation and the other ones displayed in section 3.2.2, with different-n-complex CI.

3.3. Bound-bound data

To top-up the bound-bound oscillator strength, we divide it into two parts. One is from bound states to pure bound states. i.e. between negative energy levels. We calculate all such possible transitions, but only collect the ones that are not calculated in BPRM calculations. The other part is from bound states to quasi-bound states, i.e. from negative energy bound levels to positive energy doubly excited states in the continuum. BPRM calculations treat direct photoionization and autoionization as a single unified quantum-mechanical process, as in section 3.2 that discusses direct photoionization is done. To simulate autoionizing resonances, we calculate the oscillator strengths from bound to doubly excited states, among all pairs of negative-positive energies. We consider transitions that excite an electron from L-shell to a higher one, forming a doubly excited configuration that can not be formed by combining a core configuration used in BPRM calculations with another electron. Take Fe XVIII for an example, we consider transitions from $2s^S 2p^P 3\ell$ to only $2p^5 3\ell' n\ell''$, where S, P are any possible non-negative integers satisfying $S + P = 6$, and ℓ, ℓ', ℓ'' can be any sub-shell in the corresponding
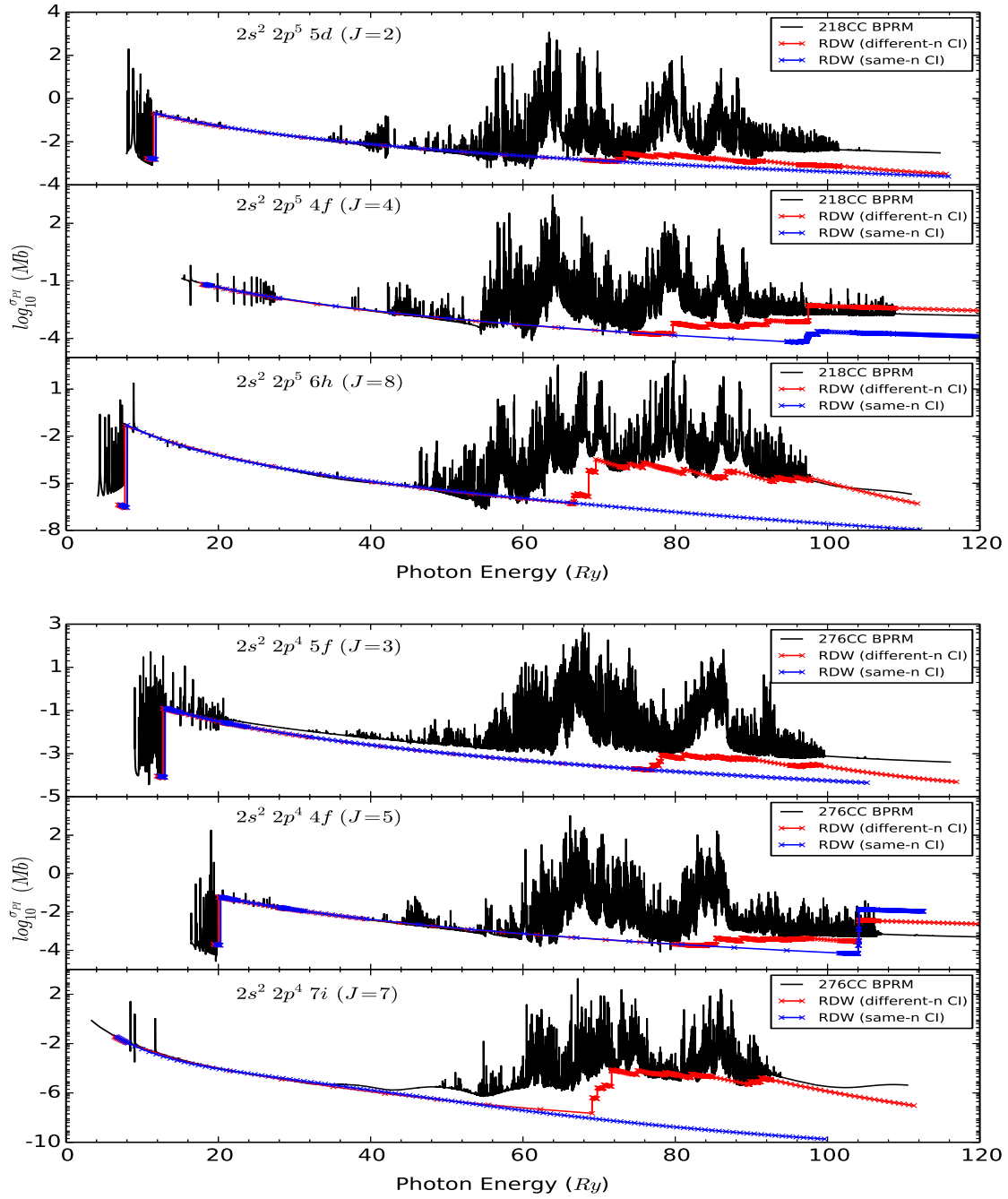
Figure 4. Different-n CI improves the background significantly, but there is still very large discrepancy in the right region of energy for some levels. BPRM (black), RDW(blue and red). "Same-n CI" refers to only same-n-complex configuration interaction is considered for core configurations, and "different-n CI" refers to both same-n- and different-n-complex configuration interaction are considered.
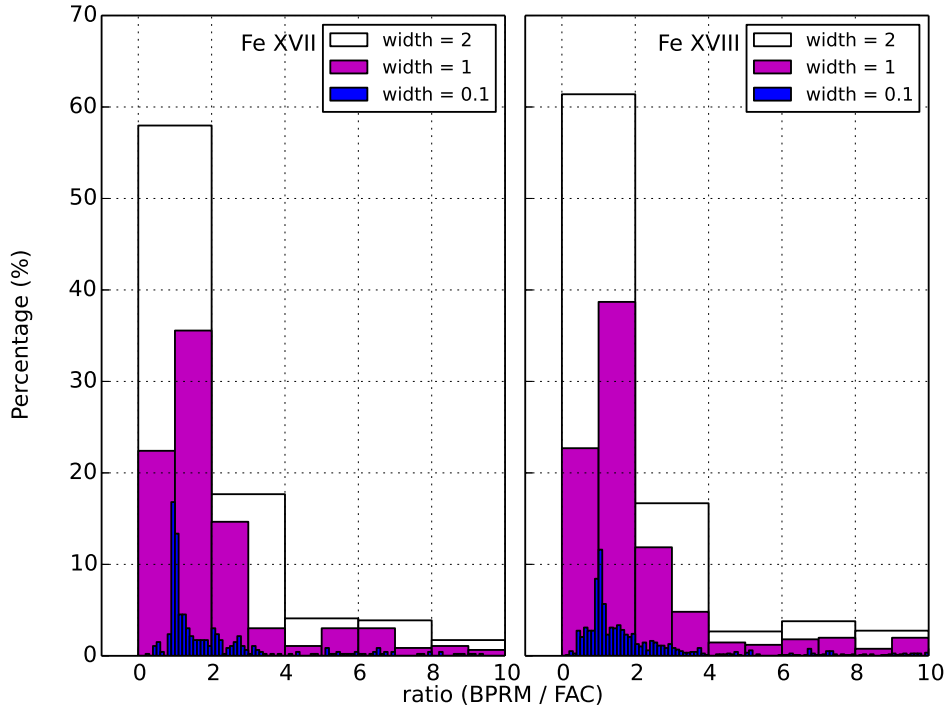
Figure 5. The distribution of the factors multiplied to RDW data in the higher energy region for Fe XVII and Fe XVIII . "width" is the width of the bins.

shell, and $n = 3 - 6$. Since $2s^2 2p^3$ and $2s2p^4$ are included in 276CC BPRM calculation, $2s^2 2p^3 3\ell' n\ell''$ and $2s2p^4 3\ell' n\ell''$ are considered naturally. Thus they are excluded in the top-up calculations.

The number of quasibound positive energy levels in the continuum is far larger than bound negative energy levels. For Fe XVII we have 587 bound levels as opposed to $\sim$72,000 positive energy levels included as top-up. For Fe XVIII we obtain 1,154 bound levels vs. $\sim$175,000 quasibound levels. All possible oscillator strengths among these large number of levels are computed and considered in opacities calculations¶.

4. Conclusion

In order to investigate the effect of convergence and completeness of RMOP data for opacities calculations, complete sets of relativistic distorted wave calculations are carried out for Fe XVII and Fe XVIII to compare with and topup the 218CC and 276CC BPRM calculations, respectively. Bound state levels are matched between BPRM and RDW calculation by comparing quantum numbers J, π, energy, and cross sections. With such

¶ We also note that oscillator strength data for transitions among quasibound positive energy levels are employed for free-free contribution to plasma broadening of autoionizing resonances, discussed in paper RMOP3
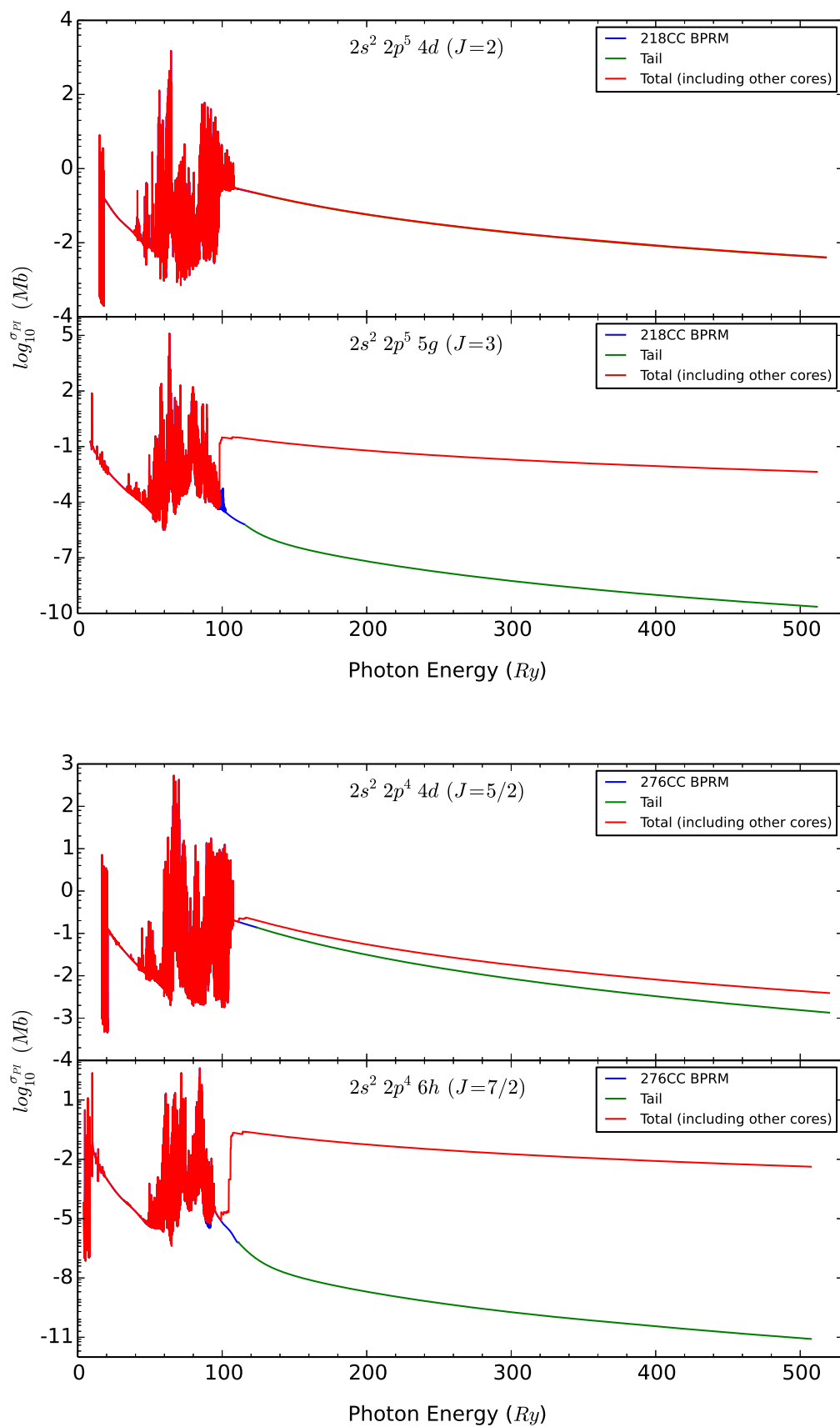
Figure 6. The photoionization cross section of the same four levels as in figure 2 are extended to higher energy region and the contribution from other core configurations

level correspondence, BPRM photoionization cross sections in the higher energy region are extended by scaled RDW data, and contribution from other core configurations up to $n = 6$ is added, to examine the effect of convergence over and above the $n \leq 4$ BPRM data. Higher bound state levels are also included with photoionization cross sections due to all core configurations up to $n = 6$. Oscillator strength data corresponding to the additional levels are also topped-up, with contribution from bound-bound and bound-quasibound transitions.

The effects of CI on photoionization cross sections are discussed, including same-n-complex and different-n-complexes, showing its significant role in reproducing the background of BPRM cross sections using RDW. However, the extensive resonance structures that dominate BPRM photoionization cross sections throughout the energy range considered can not be compared owing to their absence in the RDW data. Nevertheless, the RDW method may provide useful checks on completeness and convergence of CC-BPRM results.

We have extensively studied the correspondence and complementarity between BPRM and RDW results with a view to ascertain possible impact on opacities. However, the local-thermodynamic-equilibrium (LTE) Mihalas-Hummer-Däppen equation-of-state valid in stellar interiors yields extremely small occupation probabilities and level populations for the high energy and high (e + ion) spin-angular momenta states $nSLJ$ (discussed in paper P1), implying that the actual effect on opacities would be small. Indeed, preliminary opacities calculations indicate that Rosseland Mean Opacities are enhanced by only a few percent <5% (results to be reported elsewhere).

5. Acknowledgments

References

[1] Pradhan A K 2018 ASP Conf. Ser. 515 7
[2] Bailey J Nagayama T and Loisel G P *et al.* 2015 Nature 517 56
[3] Nahar S N Pradhan A K Chen G X and Eissner W 2011 *Phys. Rev. A* 83 053417
[4] Nahar S N and Pradhan A K *Phys. Rev. Lett.* 2016 116 235003
[5] Nahar S N and Pradhan A K *Phys. Rev. Lett.* 2016 117 249502
[6] Iglesias C and Hansen S 2017 *Astrophys. J.* 835 5

[7] Gu, M. F. 2008, Can. J. Phys., 86, 675;

[8] Seaton M J 1985 *J. Phys. B* 18 2111

[9] Nahar S N and Pradhan A K 2000 Phys. Scr. 61 675

[10] Nahar S N, Delayaye F Pradhan A K *et al.* 2000 *Astron. Astrophys. Suppl. Ser.* 144 141

[11] Eissner W, Jones M and Nussbaumer H 1974 *Comput. Phys. Commun.* 8 270

[12] The Opacity Project Team, *The Opacity Project* Vol.1 1995; Ibid. Vol. 2 1997, IOP Publishing Bristol

[13] Zhang H 1998 *Phys. Rev. A* 57 2640

[14] Zhang H Nahar S and Pradhan A 1999 *J. Phys. B* 32 1459

[15] Badnell N R and Seaton M J 2003 *J. Phys. B* 36, 4367 private communication

[16] Pradhan A K and Zhang H L 1997 *J. Phys. B* 30 L571